

# Low-Temperature Crystallization of Amorphous Silicate in Astrophysical Environments

Kyoko. K. Tanaka<sup>1</sup>, Tetsuo Yamamoto<sup>2</sup>,

Institute of Low Temperature Science, Hokkaido University, Sapporo 060-0819, Japan

and

Hiroshi Kimura<sup>3</sup>

Center for Planetary Science, Kobe 657-8501, Japan

Received \_\_\_\_\_; accepted \_\_\_\_\_

---

<sup>1</sup>Research Fellow, Institute of Low Temperature Science, Hokkaido University

<sup>2</sup>Professor, Institute of Low Temperature Science, Hokkaido University

<sup>3</sup>Associate Professor, Center of Planetary Science, Kobe University

## ABSTRACT

We construct a theoretical model for low-temperature crystallization of amorphous silicate grains induced by exothermic chemical reactions. As a first step, the model is applied to the annealing experiments, in which the samples are (1) amorphous silicate grains and (2) amorphous silicate grains covered with an amorphous carbon layer. We derive the activation energies of crystallization for amorphous silicate and amorphous carbon from the analysis of the experiments. Furthermore, we apply the model to the experiment of low-temperature crystallization of amorphous silicate core covered with an amorphous carbon layer containing reactive molecules. We clarify the conditions of low-temperature crystallization due to exothermic chemical reactions. Next, we formulate the crystallization conditions so as to be applicable to astrophysical environments. We show that the present crystallization mechanism is characterized by two quantities: the stored energy density  $Q$  in a grain and the duration of the chemical reactions  $\tau$ . The crystallization conditions are given by  $Q > Q_{\min}$  and  $\tau < \tau_{\text{cool}}$  regardless of details of the reactions and grain structure, where  $\tau_{\text{cool}}$  is the cooling timescale of the grains heated by exothermic reactions, and  $Q_{\min}$  is minimum stored energy density determined by the activation energy of crystallization. Our results suggest that silicate crystallization occurs in wider astrophysical conditions than hitherto considered.

*Subject headings:* planetary systems: protoplanetary disks- comets: general- meteors, meteoroids

## 1. Introduction

Infrared observations of various comets suggest the existence of crystalline silicates in their nuclei (Bregman et al. 1987; Molster et al. 1999). In contrast, silicate in the interstellar medium is almost or entirely amorphous, namely, free from crystallites (Li et al. 2007). It is, therefore, popular to assume that crystalline silicates observed in comets formed in the inner solar nebula (e.g., Gail 2001; Bockelee-Morvan et al. 2002; Harker and Desch 2002; Keller and Gail 2004). This is out of harmony with the composition of the gas in cometary comae, observations of which indicate the preservation of interstellar ices in the cold outer nebula (Biermann et al. 1982; Mumma 1996). As noticed by Huebner (2002), none of the thermal mechanisms proposed for silicate crystallization allows comets to retain the interstellar composition of ices in their nuclei.

Besides comets, infrared spectra tell us the presence of crystalline silicates in various kinds of object such as AGB stars, post-AGB stars, red supergiants, Herbig Ae/Be stars, and protoplanetary disks around young stellar objects. It is known that crystallization of amorphous silicate due to annealing requires temperature  $T$  above 1000 K (Hallenbeck & Nuth 1998; Fabian et al. 2000; Murata et al. 2007). It is generally considered that silicate does not crystallize below its glass transition temperature, which is 990 K for forsterite composition (Speck et al. 2008). However, infrared spectra of dust shells around evolved oxygen-rich stars exhibit the presence of several emission features of crystalline silicates in their cool dust shells ( $T < 300$  K), while silicates condense in dusty outflows with amorphous structure as evidenced by the spectra (Waters et al. 1996). Crystalline silicates are also observed in ULIRGs (ultraluminous infrared galaxies), implying that they are located in the cool, outer regions (Spoon et al. 2006). From these observational results, several researchers claim a necessity of a yet unknown crystallization process in low-temperature environments (Waters et al. 1996; Molster et al. 1999, 2001; Spoon et al.

2006; Watson et al. 2009).

Physically, crystallization is a re-arrangement of atoms irregularly placed in a solid so that the atoms occupy lattice sites; in such a configuration the solid attains the lowest internal energy. However, the atoms must overcome the energy barrier, namely, activation energy of crystallization  $E$ . In annealing, a fluctuation of thermal energy is used to overcome the energy barrier. However, a fluctuation of the thermal energy is not necessarily a requisite for crystallization. Carrez et al. (2002) and Kimura et al. (2008b) showed that amorphous silicate with forsterite composition crystallizes at room temperature when they are irradiated by electrons in a transmission electron microscope (TEM).

Recently, we have proposed another mechanism of low-temperature crystallization due to exothermic chemical reactions of reactive molecules in an organic refractory mantles surrounding an amorphous silicate core (Yamamoto & Chigai 2005; Yamamoto & Tanaka 2009; Yamamoto et al. 2009). Once the reactions are triggered by moderate heating above a few hundred kelvins, chain reactions of reactive molecules contained in the organic mantle release heat that crystallizes the surface layer of the amorphous silicate core. We estimated the degree of crystallinity to be 0.4 to 20% in volume for the concentration of reactive molecules of 1 to 10%. It was shown that the degree of crystallinity was sufficient to reproduce the observed strength of infrared features characteristic of crystalline silicates in cometary comae (Kimura et al. 2008a, 2009).

Nevertheless, we notice that the previous model of Yamamoto & Chigai (2005) and Yamamoto et al. (2009) is incomplete, because the model permits crystallization at temperatures above the melting point, although, in fact, the existence of crystalline silicate is not allowed in these temperatures. If one excludes crystallization at temperatures higher than the melting point, one would have a lower volume fraction of crystalline silicate. Furthermore, their model neglects the effect of finite particle size, namely, neglects

accumulation of the heat of chemical reactions in the particle of a finite size. In consequence, we expect that the particle-size effect increases the degree of crystallinity. These two points should be addressed in the model to properly examine the plausibility of nonthermal crystallization due to exothermic chemical reactions.

In this study, we construct a model for low-temperature crystallization of an amorphous silicate core coated with a layer of carbonaceous material, by taking into account the melting point and a finite particle size (in section 2). In view of the analyses of cometary dust and primitive interplanetary dust particles, we consider a grain having an amorphous silicate core and a mantle of carbonaceous material. Amorphous carbon is one of the main components in the carbonaceous material. (Keller et al. 1996, 2000; Kissel & Krueger 1987; Jessberger 1999). We determine the activation energies of crystallization in amorphous silicate and amorphous carbon using the revised model in comparison with two previous crystallization experiments, in which particles of (1) amorphous silicate and (2) amorphous silicate covered with a carbonaceous layer are annealed. These evaluations enable us to derive quantitative crystallization conditions. We demonstrate the validity of the model by its application to crystallization experiments due to exothermic chemical reactions demonstrated by Kaito et al. (2007) in section 3. Finally we formulate the crystallization conditions applicable to various astrophysical environments in section 4. We discuss the feasibility of nonthermal crystallization in astrophysical environments and summarize our conclusions in section 5.

## 2. Model

### 2.1. Basic equations

Cometary dust and interstellar dust are well modeled as aggregates of small grains having an amorphous silicate core and an organic refractory mantle (Kimura et al. 2003). In-situ measurements of mass spectra for dust in a coma of comet 1P/Halley show evidence of such a core-mantle structure, in which a core and a mantle are composed of silicate and organic refractory material, respectively (Kissel & Krueger 1987). A cluster of submicron grains with amorphous silicate enclosed within carbonaceous material such as amorphous carbon rich in organic material is common in primitive interplanetary dust particles of cometary origin (Keller et al. 1996, 2000; Kissel & Krueger 1987; Jessberger 1999). Because silicate crystallization in each constituent grain of the cluster occurs independently, we hereafter consider a single particle having a silicate core covered by amorphous carbonaceous material. We expect that reactive molecules have been formed by the exposure of ultraviolet radiations and high energy particles in molecular clouds and stored in the organic layer of interstellar dust.

Once the dust is heated up, the diffusion rate of reactive molecules increases and chemical reactions are triggered in the mantle layer. The energy released by the reactions raises the temperature and in turn expedites further reactions. As a consequence of the heat flow, the amorphous silicate core crystallizes. If the mantle layer is composed of amorphous carbon, the amorphous carbon may also be graphitized (Kaito et al. 2006, see also Speck et al. 2009). We take into account two types of crystallization of the silicate core.

The timescale of heat transfer in a particle is estimated to be

$$\tau_{\text{heat}} = r^2/\chi = 3 \times 10^{-8} \left( \frac{\chi}{10^{-3} \text{ cm}^2 \text{ s}^{-1}} \right)^{-1} \text{ s} \quad (1)$$

for the particle radius of  $r = 50 \text{ nm}$ . The values of  $\chi$  range from 4 to  $20 \times 10^{-3} \text{ cm}^2 \text{ s}^{-1}$  de-

pending on the temperature, compositions, and degree of crystallization (Whittington et al. 2009; Hofmeister et al. 2009). Thus we find  $\tau_{\text{heat}} < 10^{-8}$  s, which is much shorter than the crystallization timescale  $\gtrsim 10^{-5}$  s (see Appendix A). Consequently, it is safe to assume that a particle is isothermal during the crystallization process.

The energy budget of the particle at temperature  $T$  is described by

$$\frac{4}{3}\pi(a+h)^3\rho_d c_p \frac{dT}{dt} = \frac{4}{3}\pi[(a+h)^3 - a^3]\dot{\epsilon} + \Gamma_{\text{si}} + \Gamma_{\text{c}} - \Lambda_{\text{rad}} - \Lambda_{\text{coll}}, \quad (2)$$

where  $a$  is the radius of the silicate core,  $h$  is the thickness of the carbonaceous mantle,  $\rho_d (\simeq 3.0 \text{ g cm}^{-3})$  is the mean density of the particle, and  $c_p (= 1.5 \times 10^7 \text{ erg g}^{-1} \text{ K}^{-1})$  is the mean specific heat of amorphous carbon and silicate (Navrotsky 1995; Lide 1996). The first term on the right-hand side in Eq. (2) is a heating term due to exothermic chemical reactions and  $\Gamma_{\text{si}}$  is a heating rate due to deposition of the latent heat of crystallization of amorphous silicate, and  $\Gamma_{\text{c}}$  is that of amorphous carbon. For cooling processes, we take into account two cooling mechanisms due to thermal radiation  $\Lambda_{\text{rad}}$  and collisions of gas molecules surrounding the particle,  $\Lambda_{\text{coll}}$ . We assume a first order reaction, namely, the main reactions are those of reactive molecules contained in the mantle with the mantle materials.

Then the time variation of the number density  $n_A$  of the reactive molecules is expressed by

$$\frac{dn_A}{dt} = -\frac{n_A}{\tau}, \quad (3)$$

where  $\tau$  is a timescale of the reactions. The heating rate  $\dot{\epsilon}$  by the reactions is given by

$$\dot{\epsilon} = -\frac{dn_A}{dt}q_r = \frac{kQ}{\tau} \exp\left(-\frac{t}{\tau}\right). \quad (4)$$

Here,  $Q$  is the energy density stored in the carbonaceous layer given by  $Q = n_{A,0}q_r/k$ , where  $n_{A,0}$  is the initial number density of reactive molecules, and  $q_r$  is energy release per

reaction. The cooling rate due to thermal radiation,  $\Lambda_{\text{rad}}$ , is given by

$$\Lambda_{\text{rad}} = 4\pi(a + h)^2 \sigma_{\text{B}} \epsilon (T^4 - T_0^4), \quad (5)$$

where  $\epsilon$  is the efficiency of thermal emission from the surface of the carbonaceous mantle,  $T_0$  is the ambient radiation temperature, and  $\sigma_{\text{B}}$  is the Stefan-Boltzmann constant. The cooling rate  $\Lambda_{\text{coll}}$  due to collisions of ambient gas molecules of temperature  $T_0$  is given by

$$\Lambda_{\text{coll}} = 2\pi(a + h)^2 n \bar{v} k (T - T_0). \quad (6)$$

Here,  $n$  is the number density of the gas molecules,  $k$  is the Boltzmann constant, and  $\bar{v} = \sqrt{8kT_0/\mu m_{\text{a}}}$  is their mean thermal velocity, where  $\mu$  is the mean molecular weight and  $m_{\text{a}} = 1.6 \times 10^{-24}$  g is atomic mass unit.

We assume that the crystallization proceeds from the interface between the core and the mantle as is supported by crystallization experiments of grains having a silicate core and an amorphous carbon mantle (see section 2.2). This means that a crystal growth occurs through heterogeneous nucleation on the interface. Namely, crystallization of an amorphous silicate core proceeds inward in the core from the interface and graphitization of an amorphous carbon mantle proceeds outward in the mantle from the interface.

Denoting the distance of the silicate crystallization front by  $a_{\text{si}}$  and the graphitization front from the center of the particle by  $a_{\text{c}}$ , equations of the crystal growths in the silicate core and the carbonaceous mantle are given, respectively, by

$$\frac{da_{\text{si}}}{dt} = -\Omega_{\text{si}}^{1/3} \nu_{\text{si}} \exp\left(-\frac{E_{\text{si}}}{kT}\right) \left[1 - \exp\left(-\frac{q_{\text{l,si}} \Delta T_{\text{si}}}{kT^2}\right)\right], \quad (7)$$

$$\frac{da_{\text{c}}}{dt} = \Omega_{\text{c}}^{1/3} \nu_{\text{c}} \exp\left(-\frac{E_{\text{c}}}{kT}\right) \left[1 - \exp\left(-\frac{q_{\text{l,c}} \Delta T_{\text{c}}}{kT^2}\right)\right], \quad (8)$$

where  $E_i$  ( $i = \text{silicate (si), carbon (c)}$ ) is activation energy of crystallization,  $\Omega_i$  is volume of the unit cell,  $\nu_i \sim 10^{13} \text{ s}^{-1}$  is vibration frequency of the lattice. In the square bracket,  $q_{\text{l,si}}$  is latent heat of crystallization from the melt per unit cell of silicate,  $q_{\text{l,c}}$  is that of



graphitization from amorphous carbon,  $\Delta T_i \equiv T_{e,i} - T$  is the supercooling, in other words, the temperature difference between a temperature  $T_{e,i}$  of the transition from the melt or the amorphous state to the crystal in equilibrium and the temperature  $T$  in concern. The the square-bracket factors indicate the correction near the melting temperature and almost equal unity at temperatures except near the melting temperature. The heating rates due to deposition of the latent heat of crystallization are expressed by

$$\Gamma_{\text{si}} = -4\pi a_{\text{si}}^2 \frac{q_{\text{l,si}}}{\Omega_{\text{si}}} \frac{da_{\text{si}}}{dt}, \quad \Gamma_{\text{c}} = 4\pi a_{\text{c}}^2 \frac{q_{\text{l,c}}}{\Omega_{\text{c}}} \frac{da_{\text{c}}}{dt}. \quad (9)$$

## 2.2. Determination of activation energy of graphitization

First we shall derive the activation energies of crystallization in amorphous silicate and amorphous carbon, (i.e.,  $E_{\text{si}}$  and  $E_{\text{c}}$ ), by applying the model described in the previous section to crystallization experiments on submicrometer-sized grains having an amorphous silicate core and an amorphous carbon mantle. The values of the activation energies will be used in the analysis of the more sophisticated experiment of crystallization by Kaito et al. (2007). The upper panel of Fig. 1 shows a schematic picture of the crystallization experiments of amorphous silicate by Kaito et al. (2006, 2007). Kaito et al. (2006) performed an annealing experiment on amorphous silicate particles ( $\sim 50$ -100 nm in diameter) covered with an amorphous carbon layer ( $\sim 20$ -30 nm). In this experiment (which we call Exp. 1 hereafter), the crystallization of the amorphous silicate core of forsterite composition was observed at the ambient temperature of 870 K in vacuum, which is 200 K lower than the case for bare silicate grains (Fabian et al. 2000; Kamitsuji et al. 2005). The amorphous carbonaceous layer was also graphitized. Kaito et al. (2006) also found that the crystallization in both the silicate core and the carbon mantle proceeded from the interface between the core and the mantle. It might seem curious that the ‘‘crystallization temperature’’ of 870 K is lower than the glass transition temperature  $\sim 990$  K for amorphous silicate of forsterite composition

(Speck et al. 2008). Actually, crystallization of the amorphous silicate core occurs above the glass transition temperature in Exp. 1 as well. Indeed, our analysis of Exp. 1 shows that crystallization of amorphous silicate occurs around 2000 K in a short time because of a rapid temperature elevation in the grain due to graphitization of the amorphous carbon mantle followed by the cooling (see Fig. 3).

Sublimation of the grains is negligible even though they suffer temperatures as high as 2000 K. We shall show this by comparing sublimation and cooling timescales. The sublimation timescale is estimated by

$$\tau_{\text{sub}} = \left[ \left( \frac{1}{a+h} \right) \left( \frac{d(a+h)}{dt} \right) \right]^{-1} = \frac{\rho_d(a+h)}{F_e}, \quad (10)$$

where  $F_e$  is the sublimation rate given by

$$F_e = \alpha P_{\text{sat}}(T) \sqrt{\frac{m}{2\pi kT}} \quad (11)$$

with  $\alpha$  being the evaporation coefficient. The vapor pressure  $P_{\text{sat}}$  is approximated by the Clapeyron-Clausius relation expressed by  $P_{\text{sat}} = P_0 \exp\{-H/(kT)\}$ , where  $P_0$  is a constant,  $H$  is latent heat of sublimation, and  $m$  is mass of the subliming molecules. On the other hand, the cooling timescale including both collisional and radiative coolings is given by

$$\tau_{\text{cool}} = \frac{4\pi(a+h)^3 \rho_d c_p T}{3(\Lambda_{\text{coll}} + \Lambda_{\text{rad}})} \simeq \frac{2\rho_d c_p (a+h)}{3(nk\bar{v} + 2\sigma_B \epsilon_e T_c^3)} \quad (12)$$

for  $T \gg T_0$ .

Figure 2 compares the sublimation and cooling timescales of a grain coated with a carbon mantle; the cooling timescales are estimated for the ambient gas pressure of 1 atm and vacuum. For the setup of the Exp. 1 (Kaito et al. 2006), we put  $a = 50$  nm,  $h = 20$  nm, and  $\mu = 29$  (Sato 2002). Because of the core-mantle structure of the grain, sublimation of the carbon mantle would occur first, for which  $H/k = 9.5 \times 10^4$  K,  $P_0 = 1.3 \times 10^{15}$  dyn  $\text{cm}^{-2}$  (Lide 1996), and  $\alpha = 1$ . We calculated the emissivity to be  $\epsilon = 0.01$  for a core-mantle

grain of  $a = 50$  nm and  $h = 20$  nm using Mie theory. Figure 2 indicates that the sublimation timescale  $\tau_{\text{sub}}$  is longer than the cooling timescale  $\tau_{\text{cool}}$  for  $T \leq 3700$  K in vacuum and  $T \leq 5200$  K at 1 atm. The temperature of the grain experienced during the heating stage is substantially lower than these temperatures (see Fig. 3 for example), thus sublimation is negligible. This is consistent with the results of the experiments that the grains suffer little sublimation.

In this section, we apply the model to Exp. 1 to derive the activation energy of amorphous carbon. We solve the energy equation of the particle given by Eq. (2) without chemical reactions in the carbon mantle ( $\dot{\epsilon} = 0$ ) and cooling due to collisions of surrounding molecules since Exp. 1 was performed in vacuum ( $\Lambda_{\text{coll}} = 0$ ).

There are two cases of crystallization of the silicate core in the present mechanism, namely, crystallization from amorphous solid or the melt (liquid). The latter case occurs if the temperature of the particle exceeds the melting point by the large heat deposition as will be shown later. In this case, the melt crystallizes in a subsequent cooling stage when the temperature becomes lower than the melting point. In general, the activation energy for crystallization  $E_{\text{si}}$  has different values for crystallization from amorphous solid and liquid. Thus we set

$$E_{\text{si}} = E_{\text{si,s}} \quad \text{for } t \leq t_{\text{m}}, \quad (13)$$

$$E_{\text{si}} = E_{\text{si,l}} \quad \text{for } t > t_{\text{m}}, \quad (14)$$

where  $t_{\text{m}}$  is time when the particle temperature reaches the melting point,  $E_{\text{si,s}}$  and  $E_{\text{si,l}}$  are the activation energies for the amorphous silicate and that of the melt, respectively. We take  $E_{\text{si,s}}/k = 39000$  K, which was obtained from the analysis of crystallization experiments of bare amorphous silicate (Fabian et al. 2000; Kamitsuji et al. 2005) (see also Appendix A). On the other hand, the value of the activation energy of liquid  $E_{\text{si,l}}/k$  is taken to be 23000 K (Tanaka et al. 2008). For other parameters, we adopt  $q_{\text{l,si}}/k = 13800$  K (Navrotsky

1995),  $q_{l,c}/k = 5100$  K (Kaito 2007),  $T_{e,si} = 2160$  K (Navrotsky 1995),  $T_{e,c} = 3915$  K (Lide 1996),  $\Omega_{si} = 7.3 \times 10^{-23} \text{ cm}^{-3}$  (Navrotsky 1995),  $\Omega_c = 8.0 \times 10^{-24} \text{ cm}^{-3}$  (Lide 1996), and  $\nu_c = \nu_{si} = 1.2 \times 10^{13} \text{ s}^{-1}$  (Fabian et al. 2000).

Figure 3 shows a typical feature of temporal variations in the temperature  $T$  of the particle and the thicknesses  $l_{si} = a - a_{si}$  of the crystallized layer in the silicate core, and that of the graphitized layer,  $l_c = a_c - a$ , in the carbon mantle at  $T_0 = 870$  K. Here we take  $E_c/k = 23000$  K, because this value reproduces the experimental results as will be shown later.

The behavior of the crystallization process is described as follows. First, graphitization proceeds in the carbon mantle, starting from the interface between the mantle and the silicate core. During the growth of the graphite layer, the latent heat deposited is gradually accumulated in the particle because the timescale of radiative cooling ( $\gtrsim 1$  s) is longer than the growth timescale of the graphite layer ( $\simeq 0.1$  to  $1$  s) at  $T < 1000$  K. This leads to a gradual increase in the temperature of the particle. The temperature rises by about  $100$  K from  $870$  K to  $1000$  K until the thickness  $l_c$  of the graphite layer becomes a few nano-meters. A slight increase in the temperature at  $t = 0.076$  s leads to rapid graphitization. For example, the growth rate of graphite at  $1000$  K is  $20$  times larger than that at  $870$  K (i.e.,  $5 \times 10^{-5} \text{ cm s}^{-1}$ ). This results in a rapid deposit of the latent heat of graphitization and in turn the temperature rise higher than the melting point of forsterite.

The rapid rise in the temperature is a sort of a positive feedback process, in which the graphitization in the carbon mantle releases the latent heat deposition and this heating accelerates graphitization. Once the graphitization of the mantle completes, the particle cools by thermal emission. When the temperature decreases below the melting point of silicate, crystallization of the silicate core begins and proceeds inward starting from the interface between the silicate core and the carbon mantle. The silicate crystallization stops

when the crystallization of amorphous silicate reaches the center of the silicate core. The timescale of silicate crystallization is about  $10^{-3}$  s. After the complete crystallization of the amorphous silicate core, the particle cools further by thermal radiation.

Figure 4 shows crystallization features with varying the values of the activation energy  $E_c$  of graphitization at two ambient radiation temperatures of  $T_0 = 770$ K and 870K. The result of Kaito et al. (2006) indicates that bare amorphous silicate does not crystallize at  $T_0 = 770$  K but does at  $T_0 = 870$  K. This fact constrains the value of  $E_c$ . Figures 4(a)-(c) show that the  $E_c$ -value of  $E_c/k < 25000$  K explains crystallization of amorphous silicate at  $T_0 = 870$  K, while Figs. 4(d)-(e) show that  $E_c/k > 21000$  K yields no crystallization at  $T_0 = 770$  K. Thus, the activation energy of amorphous carbon must lie in the range of  $21000 \text{ K} < E_c/k < 25000 \text{ K}$ .

The range of the  $E_c$ -value is also estimated by comparing the growth timescale of graphite with the cooling timescale  $\tau_{\text{cool}}$ . If the growth time is shorter than the cooling time  $\tau_{\text{cool}}$ , amorphous carbon can be graphitized. Therefore, the condition of the graphite growth is:

$$\frac{h}{da_c/dt} < \tau_{\text{cool}}, \quad (15)$$

which leads with the use of Eq. (8) to

$$\frac{E_c}{k} < T \ln \left( \frac{\nu_c \tau_{\text{cool}} \Omega_c^{1/3}}{h} \right) = 23000 \text{K}, \quad (16)$$

where we set  $T = 870$  K and  $\tau_{\text{cool}} = 1$  s in obtaining the value of  $E_c$  on the right-hand side. In the same way, the condition of no graphite formation at 770 K is given by  $E_c/k > 19000$  K. The range of  $E_c$  thus estimated is consistent with the range of  $E_c$  constrained from Fig. 4.

From detailed calculations as shown in Fig. 4, we find that the range of  $E_c$  to explain the experimental results is

$$21300 \text{ K} < E_c < 23600 \text{ K}. \quad (17)$$

In what follows, we use  $E_c = 23000 \text{ K}$  as a standard value of the activation energy of graphitization.

### 3. Low-Temperature Crystallization in Laboratory Conditions

#### 3.1. Example of low-temperature crystallization

Kaito et al. (2007) performed another experiment on crystallization of amorphous silicate particles coated with amorphous carbonaceous layers (see the lower panel of Fig. 1). In contrast with Exp. 1, however, the carbon coating was done in a  $\text{CH}_4$  atmosphere of its pressure of  $10^{-3} \text{ Torr}$  (which we call Exp. 2 hereafter). The sample was observed by TEM after exposure to the air of the pressure of 1 atm. They found crystallization at room temperature ( $\sim 300 \text{ K}$ ) near the interface of the silicate core and the carbon layer. The crystallization time is less than one minute in the air (Kaito, private communication). They consider that heat of oxidation of methane reacting with oxygen in the air graphitized the amorphous carbon layer and the latent heat of graphitization in turn induces crystallization of the amorphous silicate core of the particles.

To clarify the conditions of crystallization due to exothermic reactions, we solve the equations of the model described in section 2 taking into account exothermic reactions and cooling due to collision of ambient air molecules at  $T_0 = 300 \text{ K}$  and the pressure of 1 atm. Figures 5 and 6 show a few examples, indicating time variations of the temperatures and the thicknesses of the crystalline silicate and graphite layers. In these figures, the radius of a silicate core and the carbon mantle thickness are the same as in Exp. 1, (i.e.,  $a = 50 \text{ nm}$  and  $h = 20 \text{ nm}$ ). Figure 5 are those for  $\tau = 5 \times 10^{-8} \text{ s}$  and (a)  $Q = 1.1 \times 10^{27} \text{ K cm}^{-3}$ , (b)  $1.0 \times 10^{27} \text{ K cm}^{-3}$ , and (c)  $0.9 \times 10^{27} \text{ K cm}^{-3}$ . In contrast to the case of Exp. 1, heat of

reactions of molecules ( $\text{CH}_4$  in Kaito et al. (2007)) contained in the carbon mantle with air leads to gradual rise in the temperature at the first stage and triggers graphitization of the carbon mantle. Heat released in graphitization leads further temperature rise above the melting point of silicate as seen in Figs. 5(a)-(b).

Silicate crystallization is observed in the subsequent cooling below the melting temperature. Note that the timescale of these processes is much shorter than that in Exp. 1 because the cooling of the particle is determined by the collisions of air molecules in Exp. 2. For Fig. 5(a)-(b), the thickness of crystalline layer of silicate is about 7 nm. The thickness of the silicate crystalline layer is consistent with the experimental results, which are shown by the bars with arrows in the bottom panels in Fig. 5. On the other hand, no silicate crystallization is observed in Fig. 5(c). This is because the stored energy density  $Q$  is insufficient for the temperature to rise above the melting temperature. From the calculations with varying  $Q$  by a finer step, we find that  $Q \geq 1.0 \times 10^{27} \text{ K cm}^{-3}$  is necessary for silicate to crystallize. In Fig. 6, we set  $Q = 1.0 \times 10^{27} \text{ K cm}^{-3}$  and varied the reaction timescale: (a)  $\tau = 5 \times 10^{-9} \text{ s}$ , (b)  $5 \times 10^{-8} \text{ s}$ , and (c)  $2 \times 10^{-7} \text{ s}$ . We find that  $\tau < 5 \times 10^{-8} \text{ s}$  is necessary for silicate crystallization. Both conditions of  $Q \geq 1 \times 10^{27} \text{ K cm}^{-3}$  and  $\tau < 5 \times 10^{-8} \text{ s}$  are necessary for silicate crystallization.

### 3.2. Analysis of Exp. 2

We give analytical consideration of Exp. 2 and estimate a minimum value of the stored energy density  $Q$  for inducing crystallization of the silicate core in the conditions of Exp. 2. Since cooling of the particle is determined by collisions of air molecules in Exp. 2, the timescale of the cooling is given by

$$\tau_{\text{cool}} = \frac{4\pi(a+h)^3 \rho_d c_p T}{3\Lambda_{\text{coll}}} \simeq \frac{2\rho_d c_p (a+h)}{3nk\bar{v}} \quad (T \gg T_0), \quad (18)$$

which is about  $10^{-6}$  s at  $T \simeq 1000$  K. This timescale is much shorter than the timescale of the crystallization of amorphous silicate, which is longer than  $10^{-5}$  s (see Appendix A). Therefore, crystallization from the solid amorphous silicate is impossible in the conditions of Exp. 2. However, once amorphous silicate melts, crystallization is possible since crystallization from the melt is easier than from the amorphous solid. The timescale of crystallization from melting particles  $\tau_{\text{cry}}$  is estimated from

$$\tau_{\text{cry}} = \frac{a}{da_{\text{si}}/dt} \quad (19)$$

of which the minimum value is about  $10^{-6}$  s at  $T \sim 2000$  K. This timescale is on the same order of magnitude as the cooling time in Exp. 2.

As shown in the previous section, graphitization of amorphous carbon expedites crystallization of the silicate core. The amorphous carbon mantle crystallizes after the temperature increases due to chemical reactions in the mantle. From Eq. (2), the time variation of the temperature before graphitization (i.e.,  $\Gamma_{\text{si}} = \Gamma_{\text{c}} = 0$ ) is given by

$$T = T_0 + \frac{kQ\tau_{\text{cool}}}{\rho_{\text{d}}c_{\text{p}}(\tau_{\text{cool}} - \tau)} \left[ 1 - \left( \frac{a}{a+h} \right)^3 \right] (e^{-t/\tau_{\text{cool}}} - e^{-t/\tau}), \quad (20)$$

where  $\tau_{\text{cool}}$  is timescale of the collisional cooling given by Eq. (18). Here we ignore the radiative cooling because the cooling is mainly due to collisions of air molecules in Exp. 2. The temperature given by Eq. (20) increases with time and reaches a maximum at

$$t = \frac{\ln(\tau_{\text{cool}}/\tau)}{1/\tau - 1/\tau_{\text{cool}}}. \quad (21)$$

The maximum temperature  $T_{\text{c}}$  is given by

$$\begin{aligned} T_{\text{c}} - T_0 &= \frac{kQ\tau_{\text{cool}}}{\rho_{\text{d}}c_{\text{p}}(\tau_{\text{cool}} - \tau)} \left[ 1 - \left( \frac{a}{a+h} \right)^3 \right] \left( \frac{\tau}{\tau_{\text{cool}}} \right)^{\tau/(\tau_{\text{cool}} - \tau)} \left( 1 - \frac{\tau}{\tau_{\text{cool}}} \right) \\ &\simeq \frac{kQ}{\rho_{\text{d}}c_{\text{p}}} \left[ 1 - \left( \frac{a}{a+h} \right)^3 \right] (\tau \ll \tau_{\text{cool}}). \end{aligned} \quad (22)$$



Note that  $T_c$  is independent of  $\tau$  and  $\tau_{\text{cool}}$  and determined only by  $Q$ . Equation (22) gives the minimum stored energy density  $Q_{\text{min}}$  given a temperature  $T_c$  that induces crystallization. Namely,  $Q_{\text{min}}$  is given by

$$Q_{\text{min}} \simeq \frac{\rho_d c_p (a+h)^3 (T_c - T_0)}{k[(a+h)^3 - a^3]}. \quad (23)$$

We get  $Q_{\text{min}} = 0.8 \times 10^{27} \text{ K cm}^{-3}$  for  $\tau_{\text{cool}} = 10^{-6} \text{ s}$  and  $T_c = 2000 \text{ K}$ , which is the graphitization temperature estimated from Eq. (15), because graphitization of the carbon mantle leads to silicate crystallization in Exp. 2. Note that this  $Q_{\text{min}}$ -value is in good agreement with the numerical calculations given in section 3.1.

#### 4. Conditions of Low Temperature Crystallization in Astrophysical Environments

The previous section focused on the analysis of Exp. 2, in which partial crystallization of a silicate core was observed when the particle was exposed to the ambient gas of its pressure of 1 atm (i.e.,  $n \sim 10^{19} \text{ cm}^{-3}$ ). For low gas densities as those in astrophysical environments, however, crystallization becomes easier than in the conditions in Exp. 2 because of inefficient collisional cooling by the ambient gas. Radiative cooling dominates the collisional cooling for very low gas densities. The gas density for which radiative and collisional coolings become comparable is estimated from  $\Lambda_{\text{rad}} = \Lambda_{\text{coll}}$  to be

$$n = \frac{\sigma_B \varepsilon_e}{k\bar{v}} T^3 = 1.4 \times 10^{13} \left( \frac{\varepsilon_e}{0.01} \right) \left( \frac{\mu}{2.2} \right)^{1/2} \left( \frac{300 \text{ K}}{T_0} \right)^{1/2} \left( \frac{T}{1000 \text{ K}} \right)^3 \text{ cm}^{-3} \quad (24)$$

for  $T \gg T_0$ , where  $\mu = 2.2$  is the mean molecular weight of a gas of the solar composition (Asplund et al. 2006). As will be shown later (Figs. 7 and 8), complete crystallization of the silicate core is realized for the gas densities lower than that estimated above, unless the stored energy density  $Q$  is so small or the reaction timescale  $\tau$  is so long to realize the crystallization.

We consider two possible processes of crystallization induced (A) by graphitization followed by chemical reactions in the mantle, and (B) reactions alone. The case (B) is considered to clarify the effect of the reactions without pre-heating played by the amorphous carbon mantle in Exp. 2. Actual situations may be situated between these two possibilities depending on the amorphousness and the composition of the mantle.

First we consider the case (A). We carry out numerical calculations with varying the ambient gas density, the stored energy density  $Q$ , and the reaction timescale  $\tau$  and explore the crystallization conditions. Figure 7 summarizes the result as a function of the number density of ambient gas molecules, showing the ranges of  $Q$  (the upper panel) and  $\tau$  (the lower panel), in which amorphous silicate particles crystallize. It should be noted that, as the gas density decreases, the regions of  $Q$  and  $\tau$  inducing the crystallization widely extend to small  $Q$  and long  $\tau$ . This extension is caused by the slow cooling due to inefficient collision frequency of the ambient gas. Complete crystallization of the silicate core is possible for the gas density  $n \leq 10^{18} \text{ cm}^{-3}$  (depending on the stored energy density  $Q$  and the timescale of the reactions  $\tau$ ); the gas density in Exp. 2 is found to be marginal and results in partial crystallization of the silicate core.

Next we explore the case (B) of crystallization induced by chemical reactions alone. Figure 8 shows the result of the numerical calculations. The overall tendency is the same as in the case (A). Namely, the ranges of  $Q$  and  $\tau$  yielding the crystallization extend to the regions of small  $Q$  and long  $\tau$  with decreasing the gas density. Compared to the case (A) shown in Fig. 7 quantitatively, the minimum value of  $Q$  required for the crystallization increases about twice of that in the case (A). In addition, partial crystallization occurs even for low gas densities. For  $n \lesssim 10^{13} \text{ cm}^{-3}$ , partial crystallization occurs in the range of  $0.8 \lesssim Q \lesssim 1.1 \times 10^{27} \text{ K cm}^{-3}$ , while complete crystallization occurs for  $Q \gtrsim 1.1 \times 10^{27} \text{ K cm}^{-3}$ .

We formulate the crystallization conditions that reproduce the numerical results shown in Figs. 7 and 8. The condition for the crystallization to occur is given by

$$Q > Q_{\min} \quad \text{and} \quad \tau < \tau_{\text{cool}}, \quad (25)$$

where  $\tau_{\text{cool}}$  is the cooling timescale of the grain and  $Q_{\min}$  is the minimum stored energy density to induce crystallization. The minimum stored energy density  $Q_{\min}$  is given by Eq. (23), in which  $T_c$  depends on the case (A) or (B). In the case (A), crystallization of the amorphous silicate core is induced by graphitization of the amorphous carbon mantle, and the temperature  $T_c$  is estimated from the graphitization condition (15) expressed as

$$T_c = \frac{E_c}{k} \left[ \ln \left\{ \frac{2\Omega_c^{1/3} \nu_c \rho_d c_p}{3(kn\bar{v} + 2\sigma_B \varepsilon_e T_c^3)} \left( \frac{a}{h} + 1 \right) \right\} \right]^{-1} \quad (T_c \gg T_0). \quad (26)$$

The solid line in the upper panel of Fig. 7 shows  $Q_{\min}$  with  $T_c$  determined from Eq. (26).

In the case (B),  $T_c$  is estimated from the relation that

$$T_c = \frac{E_{\text{si}}}{k} \left[ \ln \left\{ \frac{2\Omega_{\text{si}}^{1/3} \nu_{\text{si}} \rho_d c_p}{3(kn\bar{v} + 2\sigma_B \varepsilon_e T_c^3)} \left( 1 + \frac{h}{a} \right) \right\} \right]^{-1} \quad (27)$$

derived from the silicate crystallization condition that

$$\frac{a}{|da_{\text{si}}/dt|} \lesssim \tau_{\text{cool}}. \quad (28)$$

The solid line in the upper panel of Fig. 8 shows  $Q_{\min}$  using Eq. (27). One should note that both  $Q_{\min}$  thus estimated well reproduces the results of the numerical calculations. It should be pointed out that  $Q_{\min}$  does not depend on the absolute size of a grain but on the ratio between the mantle thickness  $h$  and the core radius  $a$ . The value of  $Q_{\min}$  decreases with increasing the ratio  $h/a$ . The cosmic abundance of elements puts a constraint on the ratio  $h/a$  to range from 0.3 to 0.5 (Kimura et al. 2003). This implies that  $Q_{\min}$  does not depend much on  $h/a$  in astrophysical situations. We used  $h/a = 0.4$  as a standard value in this study.

A maximum value of reaction timescale  $\tau$  allowing crystallization is given by  $\tau_{\text{cool}}$  (see Eq. (25)). The dot-dashed lines in the lower panels of Figs. 7 and 8 show  $\tau_{\text{cool}}$  given by Eq. (12) as a function of the gas density  $n$ . The cooling time becomes constant for  $n \leq 10^{13}$   $\text{cm}^{-3}$ , for which density the cooling is almost due to thermal radiation from the particles. The difference in  $\tau_{\text{cool}}$  is small in cases (A) and (B). One should note that  $\tau_{\text{cool}}$  reproduces the boundary of the crystallization region in the  $n$ - $\tau$  plane, indicating that the condition Eq. (25) works.

## 5. Discussion

We have constructed a theoretical model for low-temperature crystallization induced by exothermic chemical reactions in submicrometer-sized grains having a silicate core and a carbonaceous mantle. The validity of our model is proved by its application to the results of laboratory experiments on crystallization of amorphous silicate grains by Kaito and his colleagues. This enables us to formulate crystallization conditions of amorphous silicate in low-temperature environments using the stored-energy density  $Q$  and the reaction timescale  $\tau$ , irrespective of details of chemical reactions (see (25)). It should be pointed out that the conditions given in Eq. (25) are valid regardless of the grain structure, in spite of the fact that the equations are derived from the assumption of a core-mantle structure. We conclude that the low-temperature crystallization mechanism discussed in this paper should work at any dust grains unless the density  $Q$  of energy stored in the grains lies below the critical density  $Q_{\text{min}}$ .

Our results suggest that crystallization of amorphous silicate takes place in much lower temperatures than hitherto considered. As stated in section 1, crystallization of amorphous silicate needs high temperatures ( $\gtrsim 1000$  K), while the present mechanism works by moderate heating, say, of a few hundred kelvin, depending the gas density of

interest. In a protoplanetary disk, the number density of gas and its temperature at 1 AU is estimated to be  $n \sim 10^{14} \text{ cm}^{-3}$  and  $T = 300 \text{ K}$ , respectively (Hayashi 1981). One could derive the conditions for inducing silicate crystallization from Figs. 7 and 8 to be  $Q_{\text{min}} = (4 - 8) \times 10^{26} \text{ K cm}^{-3}$  and  $\tau_{\text{cool}} = 10^{-2} \text{ s}$ . This  $Q_{\text{min}}$ -value corresponds to the concentration of reactive molecules in the mantle being (5-10) % for the heat of chemical reaction  $E_r \sim 10^5 \text{ K}$ . This concentration of reactive molecules is in harmony with (1-10) % suggested in a carbonaceous mantle of interstellar dust grains (Greenberg 1976). Therefore, the nonthermal crystallization of silicate grains might come into effect in protoplanetary disks if heat of chemical reactions is deposited on the grains within a short timescale.

The minimum stored energy  $Q_{\text{min}}$  measures hardness of crystallization of silicate of various composition in the nonthermal crystallization; the larger  $Q_{\text{min}}$ , the harder the crystallization is. When the crystallization is induced by reactions (case (B) in section 4),  $Q_{\text{min}}$  is determined mainly by the activation energy of crystallization of the silicate (see Eq.(23) and Eq.(27)). For example, the activation energies of crystallization of the amorphous silicate are  $E_{\text{si}} = 39000 \text{ K}$  for forsterite composition and  $E_{\text{si}} = 42000 \text{ K}$  for that of enstatite composition (Fabian et al. 2000). The  $Q_{\text{min}}$  values are  $Q_{\text{min}} = 8 \times 10^{26} \text{ K cm}^{-3}$  for forsterite composition and  $Q_{\text{min}} = 9 \times 10^{26} \text{ K cm}^{-3}$  for enstatite composition. This indicates that the crystallization of amorphous silicate of enstatite composition is harder than that of forsterite composition. On the other hand, in the case that silicate crystallization is induced by crystallization of the amorphous mantle (graphitization for an amorphous carbon mantle) due to deposition of heat of reactions in the mantle (case (A)),  $Q_{\text{min}}$  is determined by the activation energy of crystallization of the mantle material. In this case, the hardness of silicate crystallization is independent of its composition.

As long as there is a mechanism to trigger chemical reactions in a carbonaceous layer of dust grains, amorphous silicate in the grains would suffer from low-temperature

crystallization. One of the plausible mechanisms is a flash heating of dust by shock waves, which has been proposed as a formation mechanism for chondrules found in meteorites. Once the dust is heated moderately in a shock region, diffusion of reactive molecules becomes active and will lead to chain chemical reactions. Note that the heating required for inducing crystallization of amorphous silicate is much lower than the one for chondrule formation. Collisions among dust particles, which raise the temperature in a local region of their surfaces ( $\sim$  tens of degree), may be another mechanism of flash heating. Since the above-mentioned mechanisms are most likely common to happen in protoplanetary disks, such a flash heating would trigger silicate crystallization in a protoplanetary disk.

Even if shock waves and mutual collisions are not effective enough to trigger chemical reactions, the low-temperature crystallization of amorphous silicate could be induced by spontaneous heating known as the Wigner storage mechanism in nuclear reactor engineering (Shabalin et al. 2003). It is well known for graphite irradiated by neutrons that energy stored in the form of lattice defects will be released spontaneously when the number density of the defects reaches a certain value. A similar phenomenon of spontaneous stored-energy release was observed in experimental studies of neutron-irradiated ices (Carpenter 1987; Shabalin et al. 2003; Kulagin et al. 2004). Carpenter (1987) found that the temperature of a cold solid methane moderator rises rapidly and uncontrollably when the heat loss becomes less effective after irradiation of fast neutrons into the moderator. The rapid temperature rise is due to the phenomenon that the energy stored at low temperatures in the form of reactive molecules was abruptly released from the irradiated methane by thermally activated diffusion of the molecules and their subsequent reactions.

Reactive molecules in the ice mantle of grains would form by irradiation of UV or high energy particles such as cosmic ray in the outer cold region of a protoplanetary disk or in a molecular cloud. When reactive molecules in such a grain are accumulated to a critical

number density, the heat released by the activation of reactions would induce crystallization of amorphous silicate in the grain. However, there is no observational evidence for the presence of crystalline silicate in the outer cold region of a protoplanetary disk nor in a molecular cloud. This implies either that there is an observational selection effect to obscure the presence of crystalline silicate in those environments or that the temperatures are too low to activate chain chemical reactions in the outer cold region of a protoplanetary disk and in a molecular cloud. If the latter is the case, observations with high spatial resolutions would constrain the conditions to trigger silicate crystallization and the accumulation rate of reactive molecules in low-temperature astrophysical environments.

We are grateful to C. Kaito and Y. Kimura for helpful comments and discussion and an anonymous reviewer for useful comments to improve the paper. T. Y. acknowledges support by the Grant-in-Aid for Scientific Research (21244011) from JSPS. H. K. is supported by the grants from CPS, JSPS, and MEXT Japan.

### A. Determination of the Activation Energy of Crystallization

Crystallization of an amorphous solid occurs through nucleation and growth of a crystalline nucleus. Empirically, a characteristic time scale  $\tau$  of crystallization of amorphous silicate placed at temperature  $T$  is defined by

$$\tau = \nu_{\text{si}}^{-1} \exp\left(\frac{E}{kT}\right), \quad (\text{A1})$$

where  $E$  is the effective activation energy (Hallenbeck & Nuth 1998; Fabian et al. 2000).

There are two kinds of nucleation: one is homogeneous nucleation and the other is heterogeneous nucleation in which impurities or contact interfaces act as seed nuclei for crystal growth. Homogeneous nucleation occurs in the absence of the impurities or the

interfaces. The timescale of crystallization due to homogeneous nucleation is controlled by the rate of nucleation of crystalline nuclei,  $J$ , and the growth rate  $w$  of the crystal, and is given (Kouchi et al. 1994) by

$$\tau_{\text{homo}} = \left( \frac{3}{\pi J w^3} \right)^{1/4}, \quad (\text{A2})$$

where  $J$  is a function of the interfacial energy  $\sigma$  between amorphous solid and crystals, and the activation energy of molecular diffusion  $E_{\text{si}}$  is expressed (Seki & Hasegawa 1981; Kouchi et al. 1994; Tanaka et al. 2008) as

$$J = \frac{4\pi\nu_{\text{si}}}{3\Omega_{\text{si}}} \sqrt{\frac{\beta\sigma}{\pi kT}} \exp \left\{ -\frac{E_{\text{si}}}{kT} - \frac{4(\beta\sigma)^3 T}{27q_{1,\text{si}}^2 k(\Delta T_{\text{si}})^2} \right\}. \quad (\text{A3})$$

Here,  $\Delta T_{\text{si}} \equiv T_{\text{e,si}} - T$  is the supercooling,  $\beta$  is the geometrical parameter depending on the shape of crystalline nuclei (4.8 for spherical nuclei). The growth rate of the crystal  $w$  is given by Eq. (7), i.e.,  $w = -da_{\text{si}}/dt$ .

For heterogeneous nucleation, the timescale of crystallization depends on the number of the nuclei in the amorphous solid. A picture of amorphous solid is that it consists of an ensemble of microcrystals, which have sizes of the lattice scale and are distributed in random orientations. According this view, there are already enough number of crystalline nuclei, and the timescale of (macroscopic) crystallization is given by

$$\tau_{\text{hetero}} = \frac{\Omega^{1/3}}{w}. \quad (\text{A4})$$

In this case,  $E_{\text{si}}$  corresponds to the effective activation energy  $E$  in Eq. (A1) if one ignores the melting ( $e^{-q_{1,\text{si}}\Delta T_{\text{si}}/kT^2} \ll 1$ ).

Figure 9 shows the crystallization timescales as a function of temperature. From the figure, we put constraints on the values of  $E_{\text{si}}$  and  $\sigma$ . Namely, we find that  $E_{\text{si}}/k \simeq 38000 - 39000$  K and  $\sigma < 400$  erg cm<sup>-2</sup> satisfy the results of the experiments for homogeneous nucleation, while  $E_{\text{si}}/k \simeq 38500$  K satisfies the results of the experiments for



heterogeneous nucleation. Note that the close value of the activation energy is yielded if we assume homogeneous nucleation or heterogeneous nucleation. This is because the timescale of the crystallization is mainly controlled by crystalline growth rather than nucleation in the relevant temperatures. The present value of  $E_{\text{si}}$  is in good agreement with the effective activation energy ( $E_{\text{si}}/k = 39100 \pm 400$  K) estimated by Fabian et al. (2000).

## REFERENCES

- Asplund, M., Grevesse, N., & Sauval, A. J. 2006, *Nucl. Phys. A*, 777, 1
- Biermann, L., Giguere, P. T., & Huebner W. F. 1982, *A&A*, 108, 221
- Bockelée-Morvan, D., Gautier, D., Hersant, F., J.-M. Huré, & Robert F. 2002, *A&A*, 384, 1107
- Bregman, J.D., Witteborn, F. C., Allamandola, L. J., Campins, H., Wooden, D. H., Rank, D. M., Cohen, M., & Tielens, A. G. G. M. 1987, *A&A*, 187, 616
- Carpenter, J. M. 1987, *Nature*, 330, 358
- Carrez, P., K. Demyk, H. Leroux, P. Cordier, A. P. Jones, & d’Hendecourt, L. 2002, *Meteorit. Planet. Sci.*, 37, 1615
- Fabian, D., Jäger, C., Henning, Th., Dorschner, J., & Mutschke, H. 2000, *A&A*, 364, 282
- Gail H. -P., 2001, *A&A*, 378, 192
- Greenberg, J. M. 1976, *Astrophys. Space Sci.*, 39, 9
- Hallenbeck S. L., Nuth J. A., & Daukantus, P. L. 1998, *Icarus*, 131, 198
- Harker, D. E., & Desch, S. J. 2002, *ApJ*, 565, L109
- Hayashi, C. 1981, *Prog. Theor. Phys. Suppl.*, 70, 35
- Hofmeister A. M., Whittington, A. G., & Pertermann M. 2009, *Contrib. Min. Pet.* 158, 381
- Huebner, W. F. 2002, *Earth Moon Planets*, 89, 179
- Jessberger, E. K. 1999, *Space Sci. Rev.*, 90, 91
- Kaito, C. et al. 2006, *Advances in Geosciences*, 7, 125

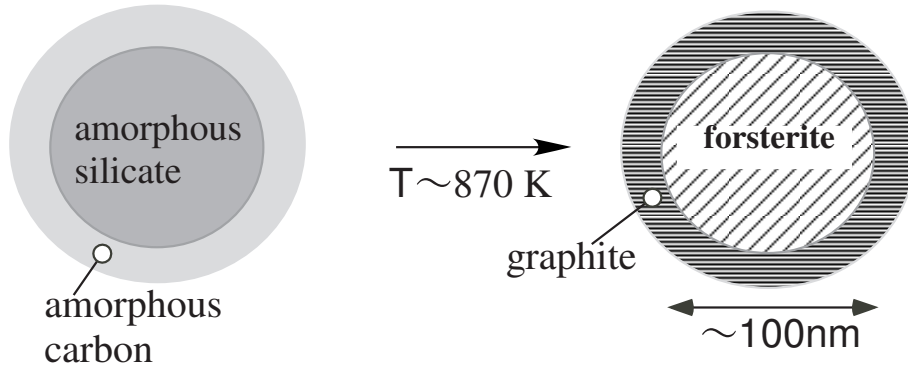
- Kaito, C. 2007, Proceeding of the third meeting of JSPS specific research on priority area  
“Extra solar planets” Dust group (in Japanese), 6
- Keller, Ch. & Gail H. -P. 2004, A&A, 415, 1177
- Kaito, C., Miyazaki, Y., Kumamoto, A., & Kimura, Y. 2007, ApJ. 666, L57
- Kamitsuji, K., Suzuki, H., Kimura, Y., Sato, Y., & Kaito, C. 2005, A&A, 429, 205
- Keller, L. P., Thomas, K. L., & McKay, D. S. 1996, Lunar Planet.Sci., 27, 659
- Keller, L. P., Messenger, S., & Bradley, J. P. 2000, J. Geophys. Res., 105, 10397
- Kimura, H., Mann, I., & Jessberger, E. K. 2003, ApJ, 583, 314
- Kimura, H., Chigai, T., & Yamamoto, T. 2008a, A&A, 482, 305
- Kimura, Y., Miyazaki, Y., Kumamoto, A., Saito, M., & Kaito C. 2008b, ApJ, 680, L89
- Kimura, H., Chigai, T., & Yamamoto, T. 2009, ApJ, 690, 482, 1590
- Kissel, J., & Krueger, F. R. 1987, Nature, 326, 755
- Kouchi, A., Yamamoto, T., Kozasa, T., Kuroda, T., & Greenberg J. M. 1994, 290, 1009
- Kulagin, E., Kulikov, S., Melikhov, V., & Shabalin, E. 2004, Nuclear Instruments and  
Methods in Physics Research Section B: Beam Interactions with Materials and  
Atoms, 215, 181
- Li, M. P., G. Zhao, & Li, A. 2007, Mon. Not. R. Astron. Soc., 382, L26
- Lide, D. R. 1996, CRC Handbook of chemistry and Physics (CRC press: Boca Raton, FL)
- Molster, F.J., et al. 1999, Nature, 401, 563

- Molster, F. J., Yamamura, I., Waters L. B. F. M., Nyman L.-Å, Käufl H.-U., de Jong T., & Loup C. 2001, *A&A*, 366, 923
- Mumma, M. J., 1996, *Nature*, 383, 581
- Murata, K., Chihara, H., Tsuchiyama, A., Koike, C., & Takakura, T. 2007, 668, 285
- Navrotsky, A. 1995, *Mineral Physics and Crystallography*, Geophysical Union, Washington
- Satoh, M. 2002, *Atmospheric circulation dynamics and general circulation models*, Springer-Praxis
- Seki, J., & Hasegawa H. 1982, *Prog. Theor. Phys.*, 66, 903
- Shabalin, E., Kulagin, E., Kulilov, & Melikhov, V. 2003, *Radiation Physics and Chemistry*, 67, 315
- Speck, A. K., Whittington, A. G., & Tartar, J. B. 2008, *ApJ*, 687, L91
- Speck, A. K., Corman, A. B., Wakeman K., Wheeler C. H., & Thompson G. 2009, *ApJ*, 691, 1202
- Spoon, H. W. W., Tielens, A. G. G. M., Armus, L., Sloan, G. C., Sargent, B., & Cami, J. 2006, *ApJ*, 638, 759
- Tanaka, K. K., Yamamoto, T., Nagashima, K., & Tsukamoto, K. 2008, *J. Crystal Growth*, 310, 1281
- Waters, L. B. F. M., et al. 1996, *A&A*, 315, L361
- Watson, D. M., et al. 2009, *ApJS*, 180, 84
- Whittington, A. G., Hofmeister, A. M., & Nebelek, P. I. 2009, *Nature*, 458, 319
- Yamamoto, T., & Chigai, T. 2005, *Highlights Astron.*, 13, 522

Yamamoto, T., Chigai, T., Kimura, H., & Tanaka, K. K. 2009, *Earth Planet Space*, in press

Yamamoto, T., & Tanaka, K. K. 2009, in *AIP Conf. Proc.* 1158, *Exoplanets and disks: their formation and diversity*, ed. T. Usuda, M. Ishii, & M. Tamura, 93

### Exp.1



### Exp.2

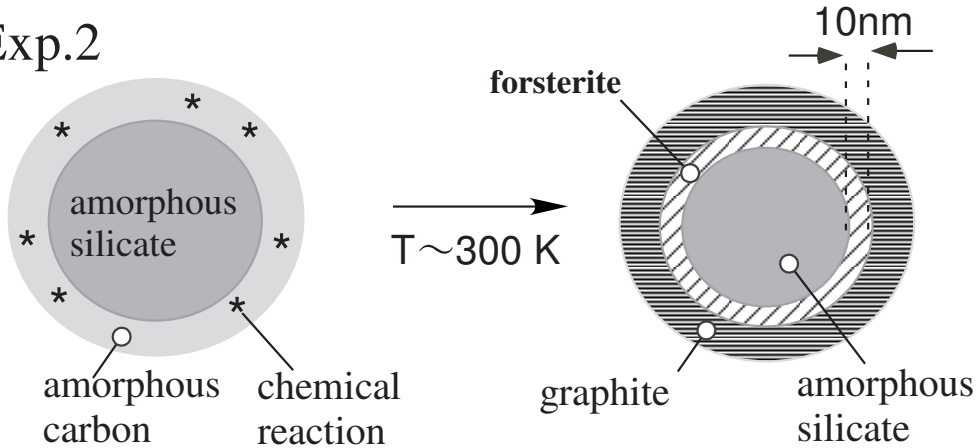


Fig. 1.— Schematic illustration of the crystallization experiments of particles having amorphous silicate core and amorphous carbon mantle. The particles used in Exp. 1 are those consisting of an amorphous silicate of forsterite composition and an amorphous carbon layer. Particles used in Exp. 2 are the same as those in Exp. 1 but contain reactive molecules (methane in the experiment by Kaito et al. (2007)) in the mantle.

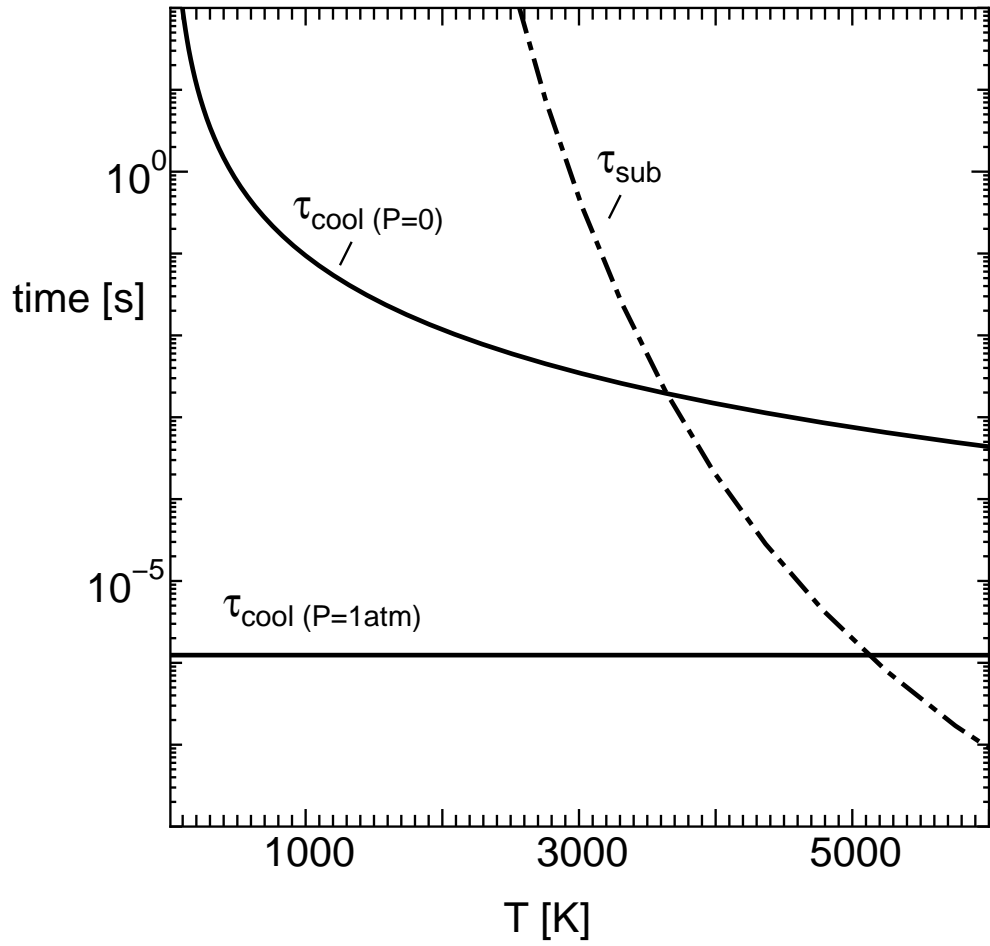


Fig. 2.— Comparison of sublimation timescale  $\tau_{\text{sub}}$  (dotted-dashed line) and cooling timescale  $\tau_{\text{cool}}$  (solid line) of a grain placed at the ambient gas pressure of 1 atm and in vacuum.

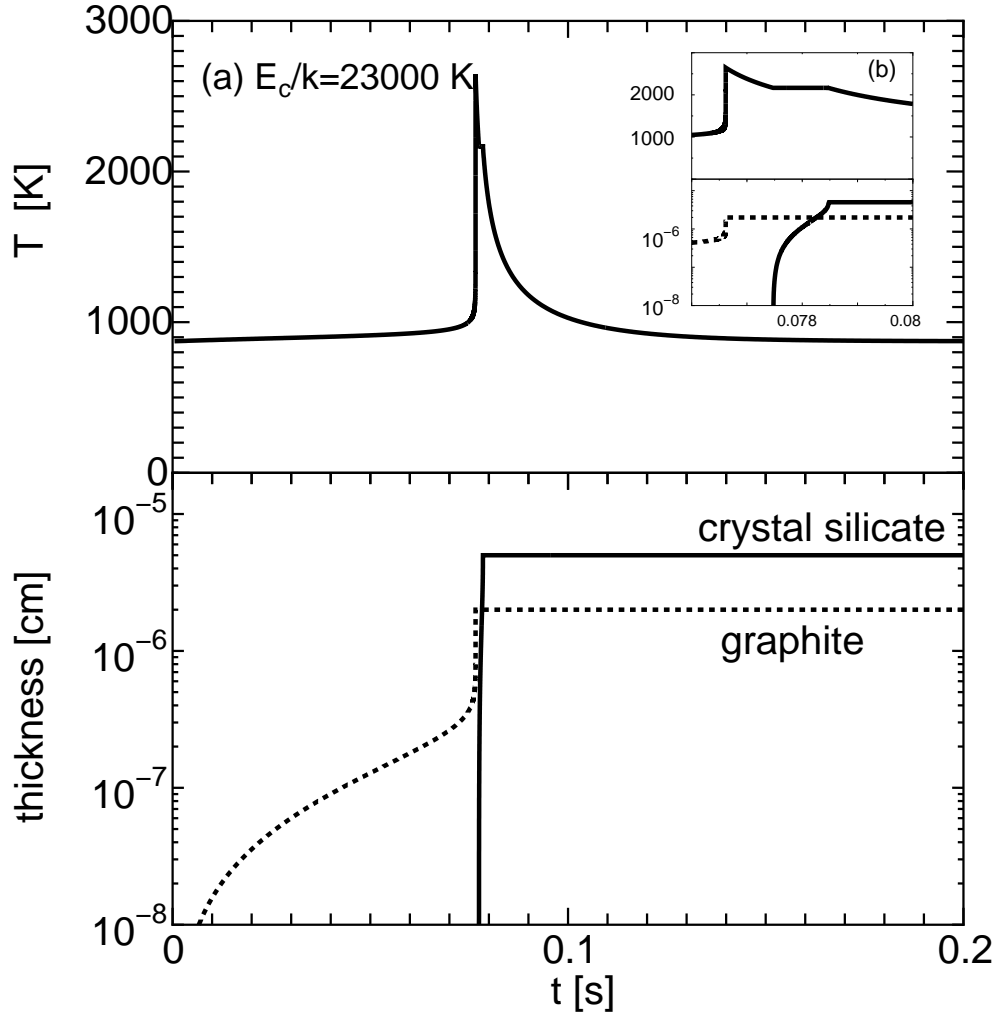


Fig. 3.— Time variations of temperature (upper panel) and thicknesses of silicate crystal  $l_{\text{si}}$  and graphite  $l_c$  (lower panel) for the setup of Exp. 1. The ambient temperature is  $T_0 = 870$  K and the activation energy of graphitization is taken to be  $E_c/k = 23000$  K. The small panel (b) is an enlargement of the part of the time interval of  $0.076 < t < 0.08$  s.



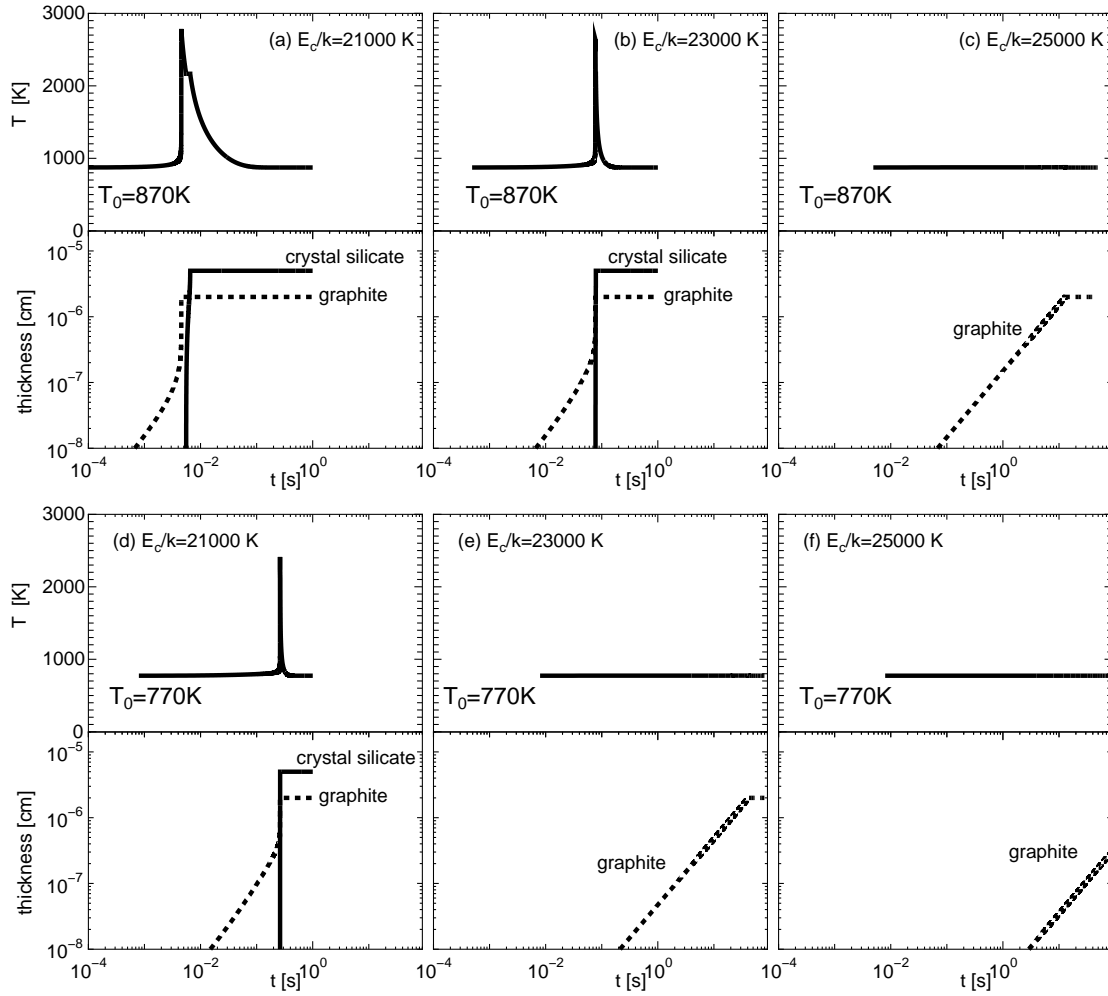


Fig. 4.— Time variations of the temperature and the thicknesses of silicate crystal and graphite for the setup of Exp. 1 conditions with varying values of the activation energy of graphitization,  $E_c$ , and the ambient temperature  $T_0$ .

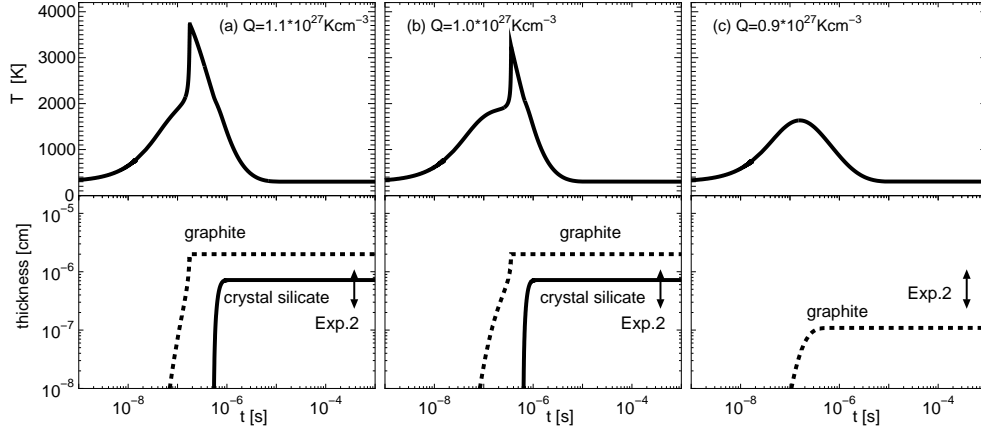


Fig. 5.— Time variations of the temperature and the thicknesses of silicate crystal  $l_{\text{si}}$  and graphite  $l_c$  for the setup of Exp. 2. In this figure we set  $\tau = 5 \times 10^{-8} \text{ s}$  and varied the  $Q$ -values: (a)  $Q = 1.1 \times 10^{27} \text{ K cm}^{-3}$ , (b)  $1.0 \times 10^{27} \text{ K cm}^{-3}$ , and (c)  $0.9 \times 10^{27} \text{ K cm}^{-3}$ . The bars with arrows indicate the range of the thickness of the crystalline silicate layer observed in Exp. 2 (Kaito et al. 2007).

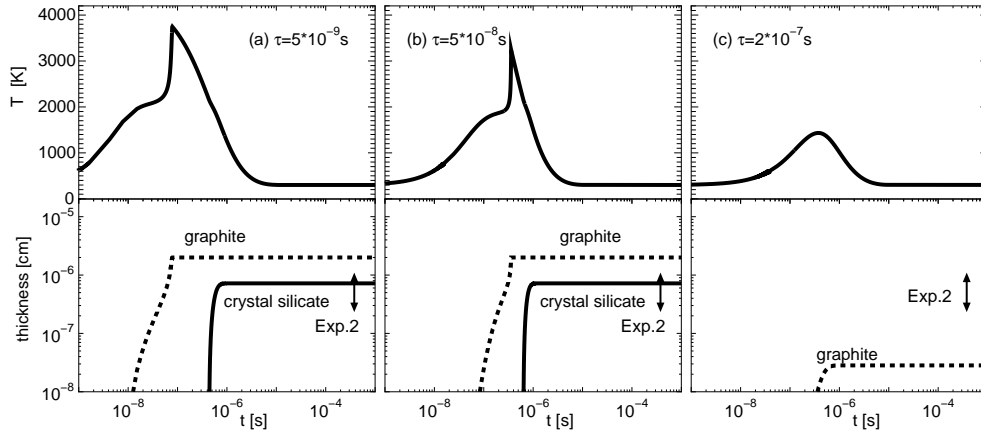


Fig. 6.— The same as in Fig. 5 but for  $Q = 1.0 \times 10^{27} \text{ K cm}^{-3}$  and (a)  $\tau = 5 \times 10^{-9} \text{ s}$ , (b)  $5 \times 10^{-8} \text{ s}$ , and (c)  $2 \times 10^{-7} \text{ s}$ .

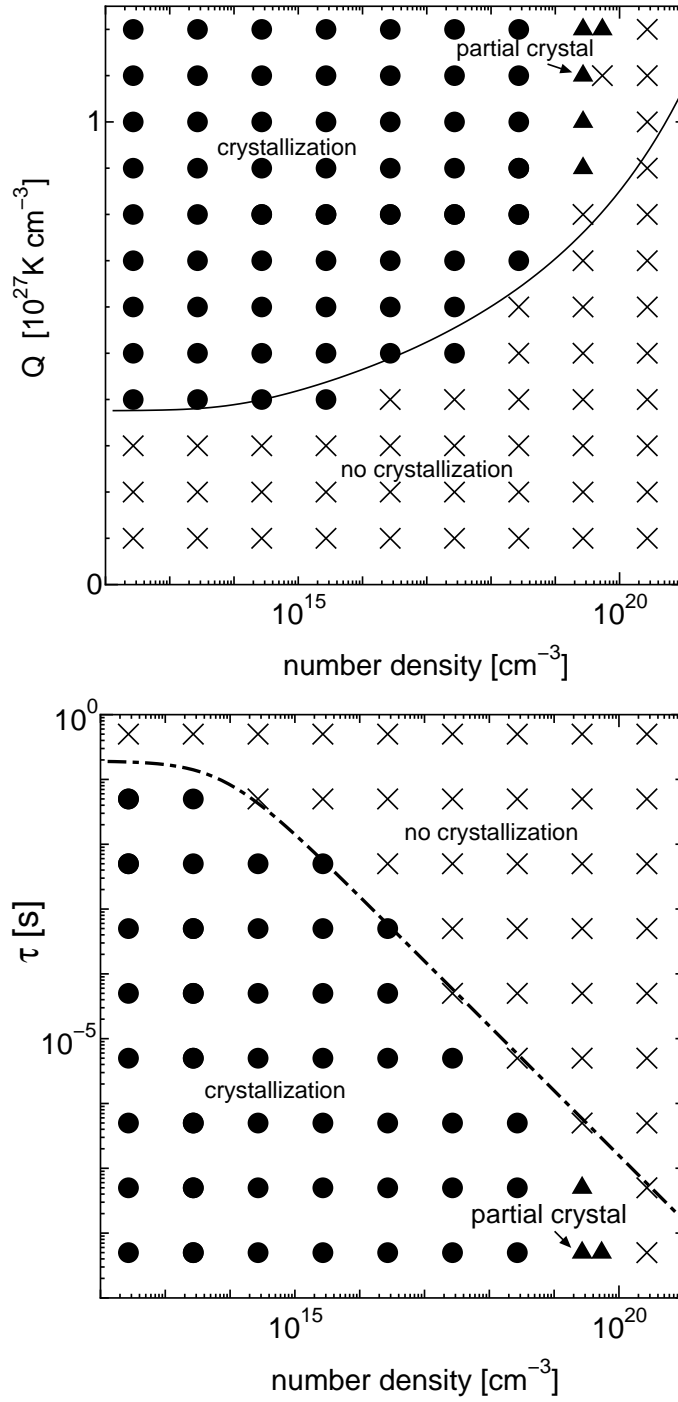


Fig. 7.— Results of calculations for nonthermal crystallization. Filled circles show complete crystallizations, triangles show partial crystallizations, and marks  $\times$  show no crystallization of amorphous silicate.

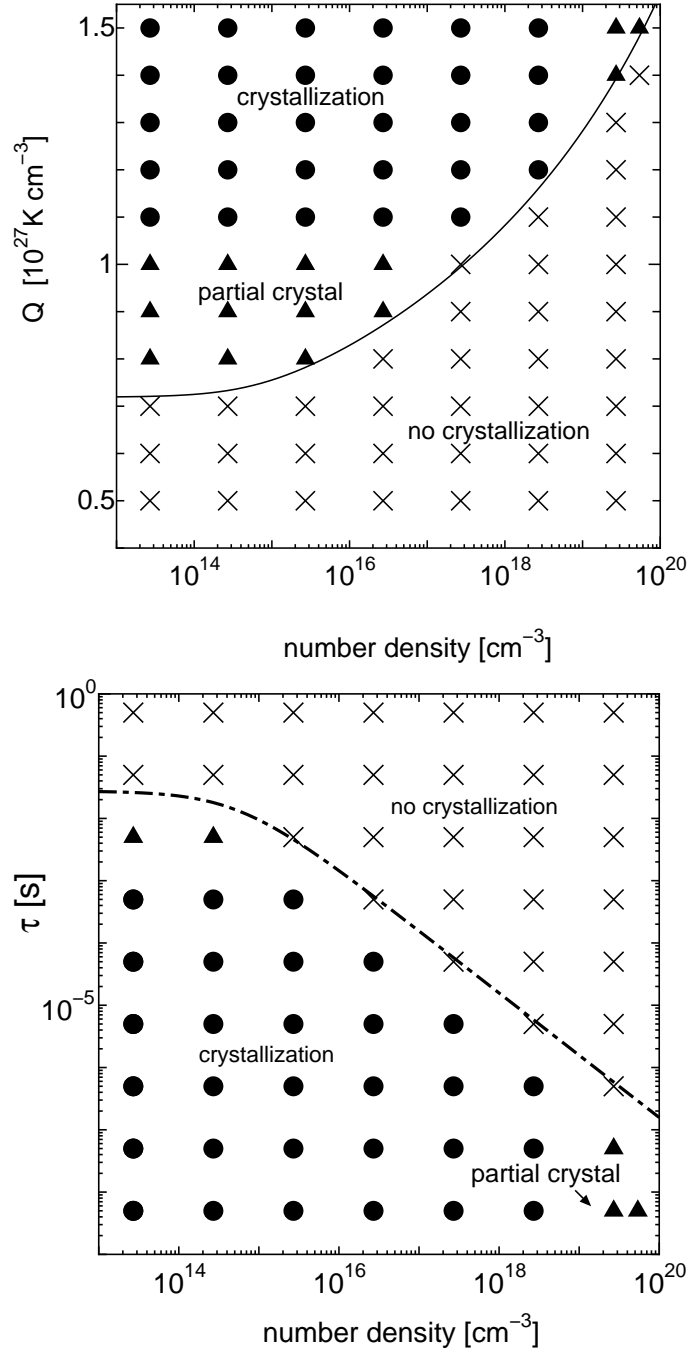


Fig. 8.— The same as Fig. 7 but for no graphitization of amorphous carbon.

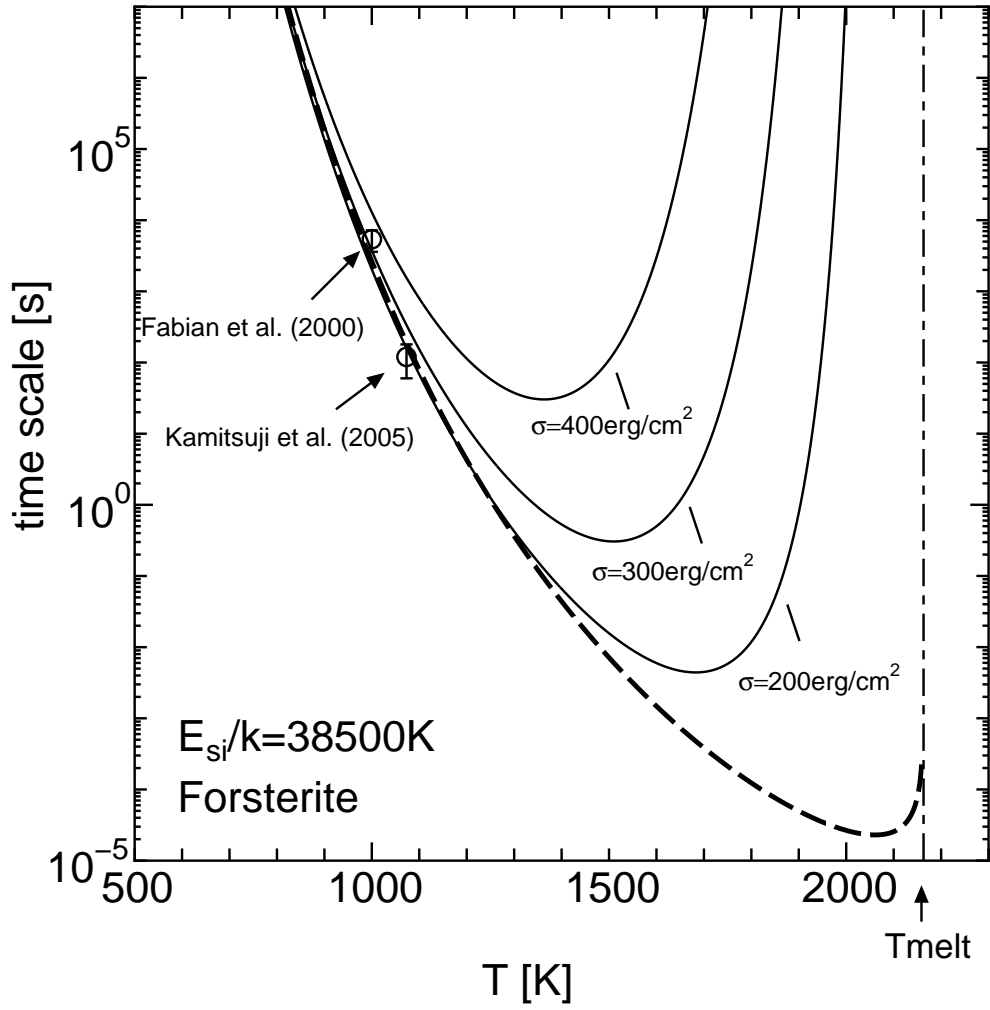


Fig. 9.— Crystallization time as a function of temperature  $T$ . Also plotted are the results of the experiments by Fabian et al. (2000) and Kamitsuji et al. (2005).